

## **Perovskite solar cells: a deep analysis using current–voltage and capacitance–voltage techniques**

DHARMADASA, I.M. <<http://orcid.org/0000-0001-7988-669X>>, RAHAQ, Y., OJO, A.A and ALANAZI, T.I.

Available from Sheffield Hallam University Research Archive (SHURA) at:  
<http://shura.shu.ac.uk/23532/>

---

This document is the author deposited version. You are advised to consult the publisher's version if you wish to cite from it.

### **Published version**

DHARMADASA, I.M., RAHAQ, Y., OJO, A.A and ALANAZI, T.I. (2018). Perovskite solar cells: a deep analysis using current–voltage and capacitance–voltage techniques. Journal of materials science: Materials in electronics.

---

### **Copyright and re-use policy**

See <http://shura.shu.ac.uk/information.html>



# Perovskite solar cells: a deep analysis using current–voltage and capacitance–voltage techniques

I. M. Dharmadasa<sup>1</sup> · Y. Rahaq<sup>1</sup> · A. A. Ojo<sup>1</sup> · T. I. Alanazi<sup>2</sup>

Received: 10 October 2018 / Accepted: 14 November 2018  
© The Author(s) 2018

## Abstract

Perovskite solar cells exhibiting ~14–15% efficiency were experimentally measured using current–voltage (I–V) and capacitance–voltage (C–V) techniques in order to extract material and device properties, and understand the action of photovoltaic (PV) operation. Deep analyses were carried out on dark- and illuminated I–V curves, and dark C–V curves. Results were compared with those of graded bandgap solar cells fabricated on inorganic n-type window layers. These analyses according to a physicist's point of view lead to understand the perovskite solar cell as a graded bandgap solar cell built on a p-type window layer. I–V and C–V results show very similar behaviour and the principle of PV action is identical. Once the stability issues with perovskites are solved, these devices have very high potential of producing next generation solar cells reaching at least mid-20% efficiency values.

## 1 Introduction

The organometal halide perovskite solar cells have acquired remarkable attention for the next generation of solar cells in the recent years due to the unique physical and electronics properties of the perovskite material [1–5]. The structural and physical properties of organometal halides  $\text{CH}_3\text{NH}_3\text{MX}_3$  were first reported by Weber in 1978 [6]. In this compound (M) represents Pb or Sn, and X represents halides, Cl, Br or I. In 2009, this material  $\text{CH}_3\text{NH}_3\text{PbX}_3$  (X = Br, I) was used as a semiconductor dye in liquid-junction dye-sensitised solar cells producing 3–4% efficiencies [7]. These efficiencies were much less than 11% efficient devices obtained during that time for Ru-based dyes. However, production of 9.7% efficient solid-state perovskite solar cells in 2012 [8], with 500 h stability triggered active worldwide research on this material. During the 6 year period (2012–2017), impressive improvement of initial efficiency increased surpassing 22% efficiency milestone [9, 10]. The perovskite solar cell efficiencies are now comparable to those of conventional

solar cells based on inorganic semiconductors such as GaAs, CdTe and CIGS.

Two main types of perovskite based solar cell configurations have been widely used in research and development stage; the conventional structure based on mesoporous structure and the inverted structure based on phenyl-C61-butyric acid methyl ester (PCBM) planar heterojunction [11]. In spite of the noteworthy attempts which have been exerted on enhancing stability issue of the perovskite solar cells, both structures of perovskite solar cells are still inadequate for commercial applications. There are real challenges of solving long-term stability and toxic nature of this device. This needs deep understanding of working of this device. This paper focuses only on the inverted structure PCBM based perovskite solar cells.

The aim of this work is the deep analysis of the devices using current–voltage (I–V) and capacitance–voltage (C–V) techniques, and extract the properties of the rectifying device structure and the material. This analysis is mainly based on conventional solid-state physics principles used for inorganic semiconductors. This attempt is to contribute to the understanding of the working principles of solid-state planar perovskite devices, showing 14–15% efficient conversion efficiencies.

✉ I. M. Dharmadasa  
Dharme@shu.ac.uk

<sup>1</sup> Materials and Engineering Research Institute, Sheffield Hallam University, Sheffield S1 1WB, UK

<sup>2</sup> Department of Physics and Astronomy, University of Sheffield, Sheffield, UK

## 2 Experimental procedure

This section briefly describes how the chemicals required to make perovskite solar cells were prepared and how the device structures were fabricated.

### 2.1 Details of materials preparation and device fabrication

Perovskite solar cells with conversion efficiencies of ~15%, characterised in this work were fabricated in our laboratories as fully described in recent publications [3, 11]. The following sections briefly describe the substrate and materials preparation procedures and solar cell fabrication method.

#### 2.1.1 Substrate preparation

Glass/Indium tin oxide (ITO) substrates used in this work were thoroughly cleaned by soap solution followed by washing in de-ionised water. Nitrogen gas stream blowing was used to dry the substrates. Further cleaning process was used by sonication in ethanol and 2-propanol separately for 5 min each followed by drying in a nitrogen gas flow.

#### 2.1.2 Preparation of materials and solutions

**2.1.2.1 Poly(3,4-ethylenedioxythiophene): poly(styrene sulfonate) (PEDOT:PSS)** The PEDOT:PSS solution was passed through 0.45 µm polyvinylidene fluoride filter before using to remove any large particles of PEDOT:PSS.

**2.1.2.2 Lead iodide solution (PbI<sub>2</sub>)** 1 M PbI<sub>2</sub> solution was prepared by dissolving 461 mg of PbI<sub>2</sub> powder in 1 ml *N,N*-dimethylformamide solvent and 20 ml of diiodooctane (DIO). DIO was added into the solution to promote the dissolution of PbI<sub>2</sub>. The PbI<sub>2</sub> solution was stirred on a hot plate at 70 °C for 12 h to obtain fully dissolved and clear PbI<sub>2</sub> solution.

**2.1.2.3 Methylammonium iodide (MAI)** CH<sub>3</sub>NH<sub>3</sub>I was synthesized following the procedure reported elsewhere [8], by the chemical reaction of 27 ml methylamine solution (CH<sub>3</sub>NH<sub>2</sub> purchased from Tokyo Chemical Industry UK Ltd, 40 wt% in methanol) with 30 ml of hydriodic acid (HI 57 wt% in water, Aldrich) in a 250 ml round-bottomed flask at 0 °C in an ice bath for 2 h. This process was carried out under normal laboratory conditions. The methylamine solution was firstly added into the round bottomed flask, then the HI was added dropwise during stirring. This mixture was transferred to a rotary evaporator

at 50 °C and kept for 1 h to remove the solvents. White solid was then collected and washed several times with diethyl ether. Finally this powder (MAI) was fully dried in vacuum at 60 °C for 24 h.

**2.1.2.4 PCBM** 30 mg of PCBM was dissolved in 1 ml of chlorobenzene and stirred on a hotplate at 70 °C for 120 min. This solution was passed through a 0.45 µm polytetrafluoroethylene filter to obtain high purity PCBM solution.

**2.1.2.5 Bathocuproine (BCP)** 2 mg of BCP was dissolved in 1 ml of methanol followed by sonication of the solution for 10 min. The solution was stirred on a hotplate at 40 °C for 30 min.

### 2.2 Solar cell fabrication

The perovskite solar cells were prepared on pre-cleaned glass/ITO substrates as summarised in Fig. 1. Firstly, thin film of PEDOT:PSS was spin-coated onto the patterned film of ITO followed by thermal annealing at 140 °C for 15 min. Two step dynamic spin coated method was used to fabricate nanocrystal structure of perovskite thin film. Thin film of PbI<sub>2</sub> was spin coated at 4000 rpm for 30 s and then dried on a hotplate at 70 °C for 8 min. Then, 200 µl of methylamine iodide solution (10 mg of MAI in 1 ml 2-propanol) was dropped onto the PbI<sub>2</sub> film, left for 60 s and spun at 4000 rpm for 30 s. Subsequently, these substrates were transferred into the glovebox and thermally annealed at 100 °C for 120 min. Then, PCBM was spin coated at 2500 rpm on top of the formed perovskite film followed by heating the thin film at 100 °C for 10 min. Finally a thin film of BCP was spin coated onto PCBM film at 2500 rpm. To make the back electrical contact, thin film of gold (100 nm) was sputter coated to complete the perovskite device structure with an active area of 0.04 cm<sup>2</sup>. Approximate material layer thicknesses of this device are: PEDOT:PSS ~40 nm, perovskite ~200 nm, PCBM ~70 nm and BCP ~10 nm.

### 2.3 Device characterisation

These devices were then characterised using I–V technique under both dark and AM1.5 illuminated conditions. The I–V system was a fully automated RERA system calibrated with a reference solar cell to establish AM1.5 illuminated condition.

The devices were also characterised using a Hewlett–Packard C–V technique under dark condition. The detection signal was applied at 1 MHz to minimise the effect of defects on measured capacitance.

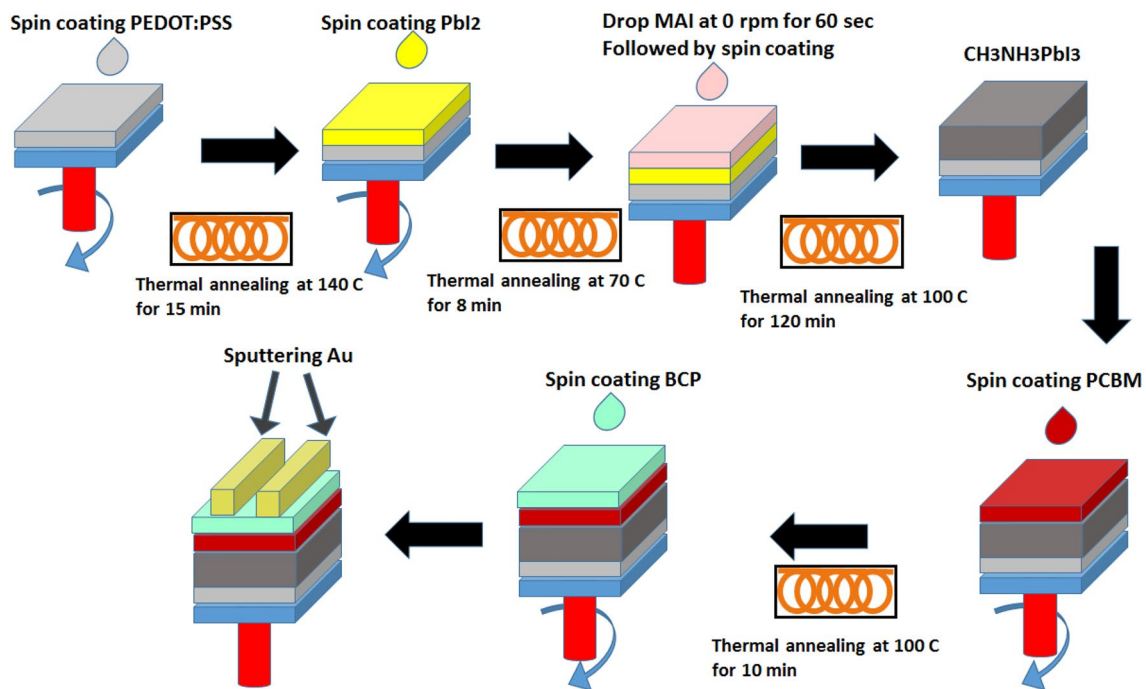


Fig. 1 Schematic diagram of perovskite solar cell fabrication procedure

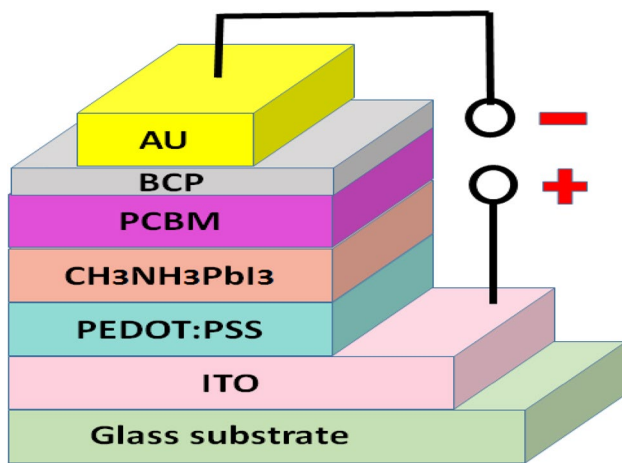


Fig. 2 Schematic diagram of the completed device structure of perovskite solar cells

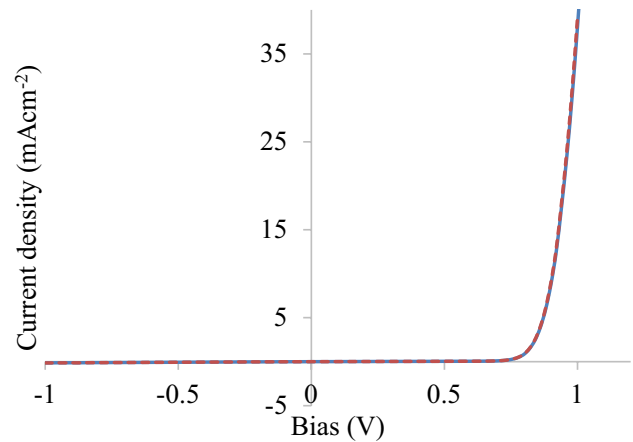


Fig. 3 Typical dark I–V characteristics plotted in a linear–linear scale representing excellent rectifying behaviour of perovskite solar cell structures

### 3 Experimental results for perovskite solar cells

#### 3.1 I–V characteristics under dark conditions

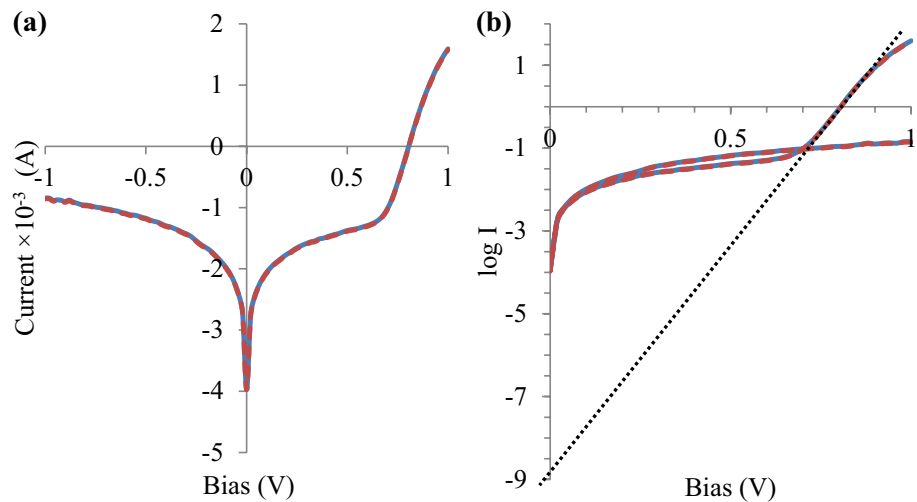
Figure 2 shows the schematic diagram of the perovskite solar cells completed after the procedures summarised in Fig. 1.

Figure 3 shows a typical dark I–V curve plotted in a linear–linear scale showing good rectification property when

voltages are applied between  $\pm 1.0$  V region. The same I–V results are plotted in log-linear scale (see Fig. 4) in order to extract more information about the device structure using the standard Eq. (1) given below for dark I–V characteristics of a rectifying contact. Extracted parameters are summarised in the first part of Table 1 for two typical devices (A and B) fabricated in this work.

The dark current as a function of applied voltage to a Schottky type rectifying contact is given by

**Fig. 4** Dark I–V plots displayed in log-linear scale for deep analysis of the rectifying perovskite device structures



**Table 1** Physical characteristics of perovskite solar cells as extracted from I–V under dark and illuminated conditions and from C–V under dark conditions

Perovskite sample	A	B
I–V under dark conditions		
$R_{sh}$ ( $\Omega$ )	$\infty$	$\infty$
$R_s$ ( $\Omega$ )	380	386
$\log(RF)$	2.6	2.5
$I_0$ (A)	$3.16 \times 10^{-9}$	$3.16 \times 10^{-9}$
$n$	1.57	1.65
$\Phi_b$ (eV)	$> 0.87$	$> 0.87$
I–V under 1.5AM illumination conditions		
$J_{sc}$ ( $\text{mA cm}^{-2}$ )	24.2	23.8
$V_{oc}$ (mV)	920	920
Fill factor	0.68	0.67
Efficiency (%)	15.1	14.7
C–V under dark conditions		
$N_D$ ( $\text{cm}^{-3}$ )	Fully depleted	$6.93 \times 10^{14}$
$C_o$ (F)	$5.11 \times 10^{-10}$	$2.49 \times 10^{-9}$
W (nm)	Fully depleted	160

height,  $k$  is Boltzmann constant,  $V$  is applied voltage and  $n$  is ideality factor of the diode.

The rectification factor (RF) of  $10^{-2.6}$  is observed for these devices. A RF is defined as the ratio of forward current to reverse current at a given voltage (say at  $V = 1.0$  V) and indicate the degree of rectification of the device. For a solar cell, RF of  $10^{-2.0}$  is adequate, but higher the value better will be the solar cell. As required for a good solar cell,  $R_{sh}$  is high ( $\infty$ ) and the series resistance is  $\sim 380 \Omega$ . Reduction of series resistance will increase the FF and hence the quality of the device will improve further. Using the diode equation valid for rectifying contacts,  $I_0$  values experimentally measured have been used to estimate potential barrier heights ( $\phi_b$ ) present in these devices. These values are in excess of 0.87 eV, and the exact value is under estimated by non-ideal “ $n$ ” values. The ideality factors of  $\sim 1.57$ – $1.65$  indicate that the charge carrier transport is due to contributions from TE over the potential barrier and the recombination process. These  $n$  values are comparable to those of rectifying devices fabricated using conventional high quality inorganic semiconductors.

### 3.2 I–V characteristics under illumination

Figure 5 shows the I–V characteristics of perovskite solar cells under AM1.5 illumination. Device parameters for two devices explored are given in the second part of the Table 1. Devices show  $\sim 15\%$  conversion efficiency with  $J_{sc} \sim 24 \text{ mA cm}^{-2}$ ,  $V_{oc} \sim 920 \text{ mV}$  and FF  $\sim 0.68$  representing a good thin film solar cell structure.

### 3.3 C–V characteristics

C–V relationship of the devices was measured under dark conditions in order to learn more about these materials and devices. The frequency of the detection signal was kept at

$$I_D = SA^*T^2 \exp\left(\frac{-e\phi_b}{kT}\right) \left\{ \exp\left(\frac{eV}{nkT}\right) - 1 \right\} \quad (1)$$

$$I_0 = SA^*T^2 \exp\left(\frac{-e\phi_b}{kT}\right) \quad (2)$$

where  $I_D$  is electric current in dark conditions,  $S$  is area of the device,  $A^*$  is effective Richardson constant for thermionic emission (TE)  $\left\{ A^* = \left( \frac{4\pi m^* e k^2}{h^3} \right) \sim 120 \left( \frac{m^*}{m_o} \right) \text{Acm}^{-2} \text{K}^{-2} \right\}$ ,  $T$  is temperature in kelvin,  $e$  is electronic charge,  $\phi_b$  is potential barrier

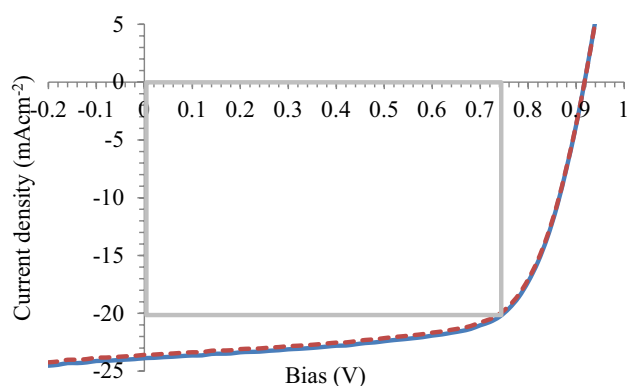


**Fig. 5** Typical I–V curve under AM1.5 illumination showing conversion efficiency of ~15%

1 MHz so that the defects within the device structure cannot respond with electric field variations and therefore minimise the effects of defects on measured capacitance. Figures 6 and 7 represent C–V and Mott–Schottky plots ( $1/C^2$  vs. V) obtained for devices A and B, and parameters obtained are summarised in Table 1.

**Fig. 6** Capacitance versus bias voltage **a** and the corresponding Mott–Schottky plot **b** for device A with ~15.1% efficiency

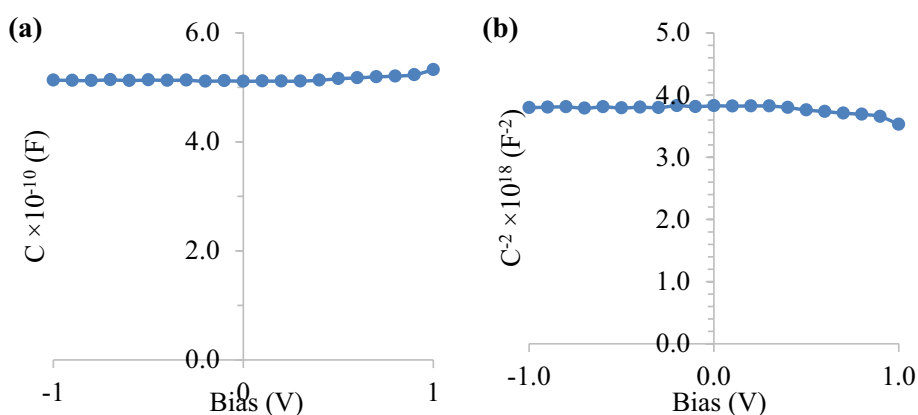
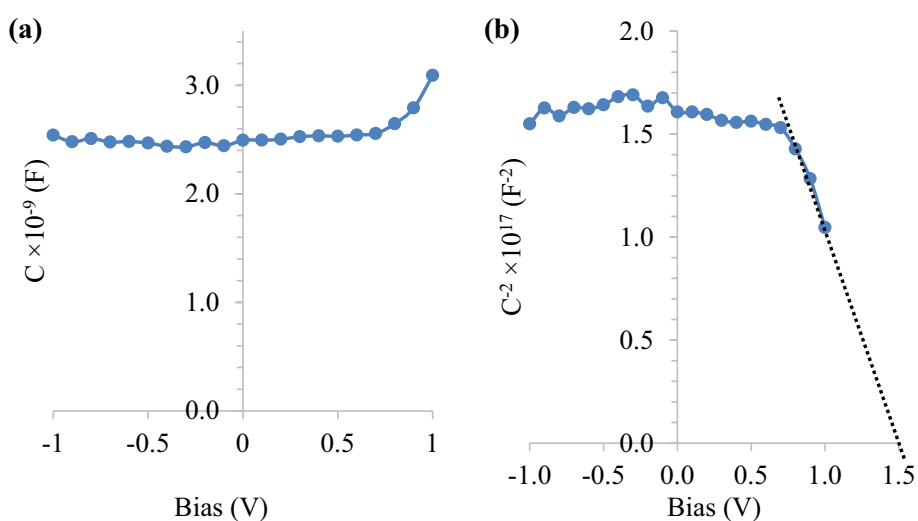


**Fig. 7** Capacitance versus bias voltage **a** and the corresponding Mott–Schottky plot **b** for device B with ~14.7% efficiency



C–V plots show that the capacitance values measured are almost constant indicating a fully depleted device. In other words, the width of the depletion region exceeds the geometrical thickness of the device. However, device B shows the increase in capacitance beyond ~0.7 V forward bias voltage and these data points have been used to approximately estimate the doping concentration of perovskite. This value is estimated to be  $\sim 6.93 \times 10^{14} \text{ cm}^{-3}$ . For these bias voltages the width of the depletion region is less than the thickness of the absorber material.

## 4 Comparison with inorganic solar cells

Before moving into a deep discussion on perovskite solar cell results, it is appropriate to briefly present similar results reported [12, 13] for graded bandgap solar cells fabricated with known inorganic semiconductors. These structures consist of three semiconducting layers and grown using electroplating to complete glass/FTO/n-ZnS/n-CdS/n-CdTe/Au solar cells. The band diagram of these solar cells is shown in Fig. 8.

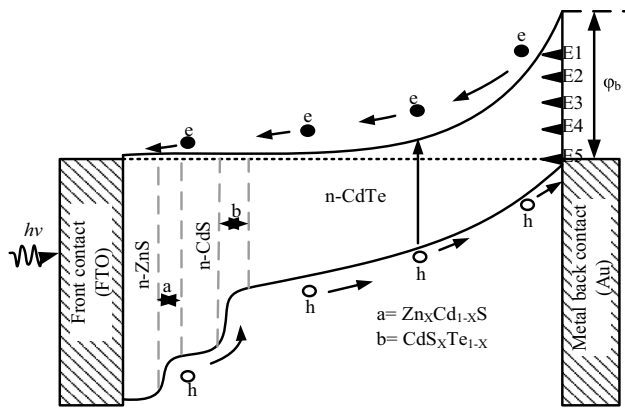
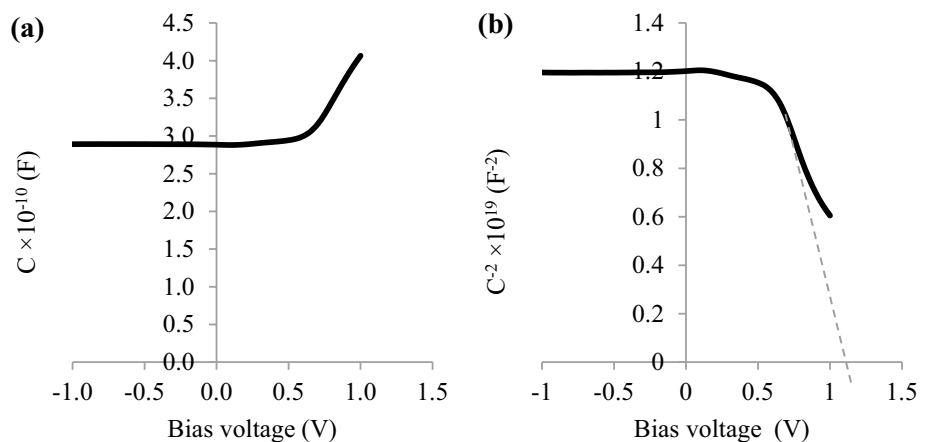


**Fig. 8** Energy band diagram of the glass/FTO/n-ZnS/n-CdS/n-CdTe/Au graded bandgap structure reported in reference [12, 13]

**Table 2** Summary of device parameters obtained by I–V and C–V techniques for glass/FTO/n-ZnS/n-CdS/n-CdTe/Au structures fabricated with electroplated materials

IV under dark conditions	
$R_{sh}$ ( $\Omega$ )	$> 10^5$
$R_s$ ( $\Omega$ )	470
log (RF)	4.8
$I_o$ (A)	$1.0 \times 10^{-9}$
$n$	1.60
$\Phi_b$ (eV)	$> 0.82$
I–V under 1.5 AM illumination conditions	
$J_{sc}$ ( $\text{mA cm}^{-2}$ )	34.1
$V_{oc}$ (mV)	730
Fill factor	0.57
Efficiency (%)	14.2
C–V under dark conditions	
$\sigma \times 10^{-4}$ ( $\Omega \text{ cm}$ ) $^{-1}$	8.82
$N_D - N_A$ ( $\text{cm}^{-3}$ )	$7.79 \times 10^{14}$
$C_o$ (F)	280
$W$ (nm)	1092

**Fig. 9** The C–V characteristics measured under dark conditions for glass/FTO/n-ZnS/n-CdS/n-CdTe/Au structures fabricated with inorganic semiconductors



#### 4.1 I–V characteristics

Typical properties of I–V characteristics under dark conditions for these devices are summarised in Table 2. By comparing results in Tables 1 and 2, the major difference is the improved RF of  $\sim 10^{4.8}$ , instead of  $\sim 10^{2.6}$  for perovskite solar cells. However, a good solar cell requires only  $\sim 10^{2.0}$  RF to have high efficiencies and therefore this is not a considerable difference to obtain efficiencies of 14–15%. All other parameters are comparable but perovskite solar cells seem to have high potential barriers in their structure.

Typical device parameters under AM1.5 illumination and the device parameters are summarised in Table 2. Device properties have some variations but the overall conversion efficiency values are comparable ( $\sim 14.2\%$ ).

#### 4.2 C–V characteristics

C–V characteristics under dark conditions are shown in Fig. 9. Comparison with Fig. 7 for these results for perovskite solar cells, behaviour is identical. The possible parameters obtained are given in Tables 1 and 2, although additional parameters have been extracted for inorganic solar cells by measuring electrical conductivity,  $\sigma$ . Overall, behaviour of two rectifying devices are very similar.

### 5 Discussion of inorganic solar cells

As reported in reference [12] and other relevant publications [13–15] glass/FTO/n-ZnS/n-CdS/n-CdTe/Au devices are graded bandgap devices built on wide bandgap n-ZnS window layers. At the back of the absorber layer (n-CdTe), Au forms a large potential barrier height ( $\phi_b$ ) due to Fermi level pinning at defect level  $E_5$  closer to the valence band. Therefore, this structure has two hetero-junctions and a large Schottky barrier at the back, connected in parallel, because



the photo-current produced by three junctions add up in the external circuit.

At zero bias, this structure is fully depleted, but when the forward bias is applied, around 0.5 V, the depletion width shrinks to approximately equal to the thickness of the absorber layer. Therefore, capacitance increases with further increase in forward bias voltage, and behave according to Mott–Schottky relationship.

In summary, the inorganic solar cells compared in this paper are graded bandgap solar cells fabricated on wide bandgap n-type window layers as published before [12–15].

## 6 Discussion of perovskite solar cell

In order to describe the perovskite solar cell through a device physicists' point of view, we have taken the LUMO and HOMO level energy values reported in the literature for materials used in this solar cell [16]. These values are summarised in Table 3, and most of the published papers use these energy level values with reference to the “vacuum level”. This approach is appropriate for theoretical calculations, for “ideal” systems. In the case of thin film solar cells, material layer thicknesses are in nm region, and therefore seriously affected by defects. This is where strong “Fermi level pinning” takes place as reported in the past [17–19]. Hence, when trying to describe these “non-ideal” systems, it is more appropriate to use the Fermi level as the reference energy level. Because of the above reason, we have used the published LUMO and HOMO energy levels only to calculate the forbidden band gaps of materials ( $E_g$ ) and these are summarised in Table 3. Also, the knowledge from the literature was used to decide the electrical conductivity type of four materials used in a perovskite solar cell. Device design or analysis of experimental results cannot be done without knowing the crucial information of “electrical conduction type”.

Taking the “Fermi level” aligned across the device as the reference, and energy band gaps and electrical conductivity types of materials shown in Table 3, it is possible to sketch the energy band diagram for perovskite solar cells. Figure 10 shows the constructed energy band diagram for the perovskite solar cells studied in this work. This is clearly a graded bandgap solar cell device fabricated on a wide bandgap

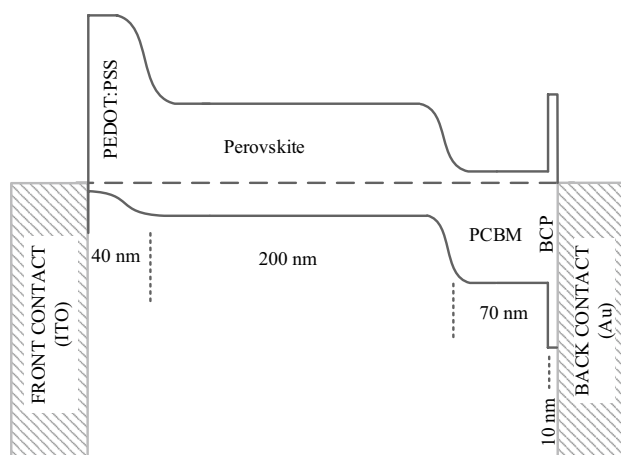


**Fig. 10** Energy band diagram of the perovskite solar cell when the “Fermi level” is taken as the reference energy level instead of the “vacuum level” (note the drawing is not to scale)

p-type window material with another three layers. Therefore, both the I–V and C–V results observed can be explained easily using the conventional photovoltaic (PV) description for inorganic materials based devices.

The structure provides a high potential barrier for electrons due to wide bandgap p-type PEDOT:PSS layer. Therefore, there is a healthy slope or an internal electric field throughout the device structure and hence photo-generated charge carriers are created, separated and collected efficiently, when illuminated. The 10 nm thick BCP insulating layer acts as an hole back diffusion barrier layer separating the electrons and holes in back and front electrical contacts in open circuit mode. This also acts as a pin-hole plugging layer to improve the performance of the device. Because of the high potential barrier created in this device structure, high  $V_{oc}$  values can be produced. This is the main reason for achieving  $V_{oc} > 1.00$  V for optimised perovskite solar cells. The 10 nm BCP layer is transparent to accelerated electrons, but acts as a barrier for thermal electrons in the back contact. Without this layer, the efficiency of the cell will be very low.

As a new approach for next generation solar cells development, the SHU group has proposed [20] and now working on graded bandgap device structures [12, 13, 21–23]. The device designs proposed are shown in Fig. 11 for both solar cells possible on p-type and n-type wide bandgap window materials.

**Table 3** Summary of properties of material layers used in the fabrication of perovskite solar cells

Material	Thickness (nm)	LUMO level (eV)	HOMO level (eV)	$E_g$ (eV)	Comments
PEDOT:PSS	40	5.4	3.5	1.9	p-type semiconductor
Perovskite	200	5.4	3.9	1.5	p-type semiconductor
PCBM	70	6.0	4.0	2.0	n-type semiconductor
BCP	10	7.0	3.6	3.4	Insulator



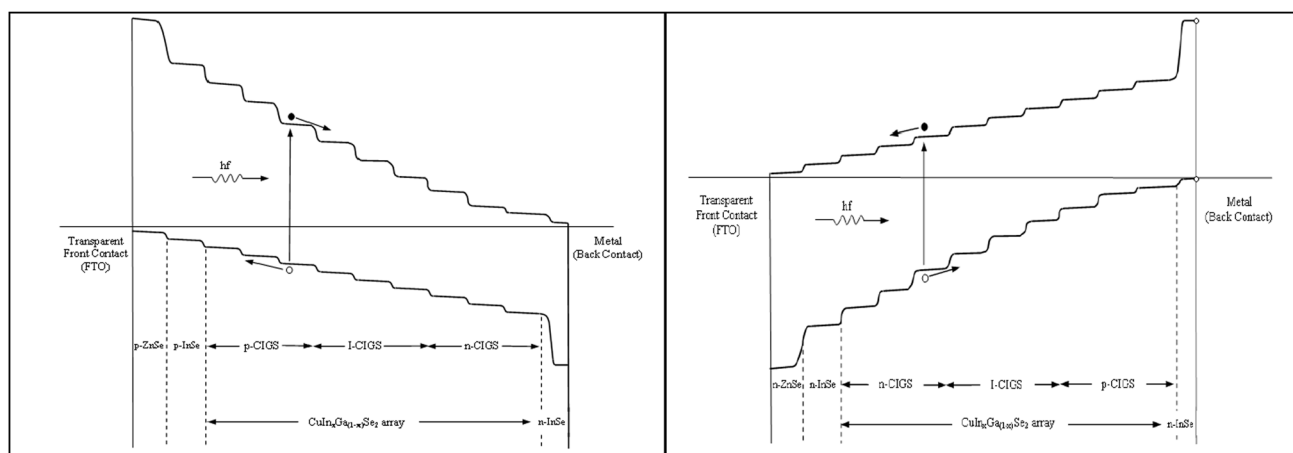


**Fig. 11** Multi-layer (~12 layers) graded bandgap solar cell structures possible on p-type and n-type window materials [21, 23]

Out of these two structures devices fabricated on p-windows are more capable of achieving high device parameters. The SHU solar energy group is currently working on both these devices but the inorganic solar cells summarized in this paper were built on n-type window materials due to the availability of materials at present. The perovskite solar cells developed to date without fully understanding the PV action, in fact are graded bandgap devices fabricated on p-type window materials. Therefore, these are capable of producing  $V_{oc} > 1.00$  V as experimentally shown using GaAs/AlGaAs system achieving 1.175 V for this parameter [21]. Once the stability issues of perovskite materials are solved, these devices should produce high efficiency and low cost thin film devices with high efficiencies in the future.

## 7 Conclusions

In this paper, 14–15% efficient perovskite solar cells have been fully analysed using I–V and C–V techniques. These results were compared with ~14% efficient inorganic solar cells fabricated with electroplated semiconductors. It has been concluded that both devices act in a similar way and represent graded bandgap devices with 3–4 solar energy material layers. Inorganic solar cell compared here is a graded bandgap device built on n-type window material and the perovskite solar cells presented here are graded bandgap devices fabricated on p-type window material. Once stable perovskite based materials are established these devices should produce high efficiency solar cells in thin film solar PV field.

**Open Access** This article is distributed under the terms of the Creative Commons Attribution 4.0 International License (<http://creativecommons.org/licenses/by/4.0/>), which permits unrestricted use, distribution, and reproduction in any medium, provided you give appropriate credit to the original author(s) and the source, provide a link to the Creative Commons license, and indicate if changes were made.

## References

1. W. Tress, M. Yavari, K. Domanski, P. Yadav, B. Niesen, J.P.C. Baena, A. Hagfeldt, M. Graetzel, Interpretation and evolution of open-circuit voltage, recombination, ideality factor and sub-gap defect states during reversible light-soaking and irreversible degradation of perovskite solar cells. *Energy Environ. Sci.* **11**, 151 (2018)
2. Q. Lin, Z. Wang, H.J. Snaith, M.B. Johnston, L.M. Herz, Hybrid perovskites: prospects for concentrator solar cells. *Adv. Sci.* **5**, 1700792 (2018)
3. Y. Rahaq, M. Moussa, A. Mohammad, H. Wang, A. Hassan, Highly reproducible perovskite solar cells via controlling the morphologies of the perovskite thin films by the solution-processed two-step method. *J. Mater. Sci.* **29**, 16426–16436 (2018)
4. L. Qiu, L.K. Ono, Y. Qi, Advances and challenges to the commercialization of organic–inorganic halide perovskite solar cell technology. *Mater. Today Energy* **7**, 169–189 (2017)
5. T. Ibn-Mohammed, S.C.L. Koh, I.M. Reaney, A. Acquaye, G. Schileo, K.B. Mustapha, R. Greenough, Perovskite solar cells: an integrated hybrid lifecycle assessment and review in comparison with other photovoltaic technologies. *Renew. Sustain. Energy Rev.* **80**, 1321–1344 (2017)
6. D. Weber,  $\text{CH}_3\text{NH}_3\text{PbX}_3$ , A Pb (II)-system with cubic perovskite structure. *Zeitschrift für Naturforsch. B* **33**, 1443–1445 (1978). <https://doi.org/10.1515/znB-1978-1214>
7. K. Akihiro, K. Teshima, Y. Shirai, T. Miyasaka, Organometal halide perovskites as visible-light sensitizers for photovoltaic cells. *J. Am. Chem. Soc.* **131**, 6050–6051 (2009). <https://doi.org/10.1021/ja809598r>
8. H.-S. Kim, C.-R. Lee, J.-H. Im, K.-B. Lee, T. Moehl, A. Marchioro, S.-J. Moon, R. Humphry-Baker, J.-H. Yum, J.E. Moser, M. Grätzel, N.-G. Park, Lead iodide perovskite sensitized all-solid-state submicron thin film mesoscopic solar cell with efficiency exceeding 9%. *Sci. Rep.* **2**, 591 (2012). <https://doi.org/10.1038/srep00591>
9. M. Saliba, J.-P. Correa-Baena, C.M. Wolff, M. Stollerfoht, N. Phung, S. Albrecht, D. Neher, A. Abate, How to make over 20% efficient perovskite solar cells in regular (n-i-p) and inverted (p-i-n) architectures. *Chem. Mater.* (2018). <https://doi.org/10.1021/acs.chemmater.8b00136>
10. M. Wong-Stringer, O.S. Game, J.A. Smith, T.J. Routledge, B.A. Alqurashy, B.G. Freestone, A.J. Parnell, N. Vaenas, V. Kumar, M.O.A. Alawad, A. Iraqi, C. Rodenburg, D.G. Lidzey,

- High-performance multilayer encapsulation for perovskite photovoltaics. *Adv. Energy Mater.* **8**, 1801234 (2018). <https://doi.org/10.1002/aenm.201801234>
11. H. Wang, Y. Rahaq, V. Kumar, A composite light-harvesting layer from photoactive polymer and halide perovskite for planar heterojunction solar cells. *Sci. Rep.* **6**, 29567 (2016). <https://doi.org/10.1038/srep29567>
  12. A.A. Ojo, H.I. Salim, I.M. Dharmadasa, The influence of ZnS crystallinity on all-electroplated ZnS/CdS/CdTe graded bandgap device properties. *J. Mater. Sci. Mater. Electron.* **29**, 13631–13642 (2018). <https://doi.org/10.1007/s10854-018-9491-4>
  13. A.A. Ojo, I.M. Dharmadasa, Analysis of the electronic properties of all-electroplated ZnS, CdS and CdTe graded bandgap photovoltaic device configuration. *Sol. Energy* **158**, 721–727 (2017). <https://doi.org/10.1016/j.solener.2017.10.042>
  14. O.I. Olusola, M.L. Madugu, I.M. Dharmadasa, Investigating the electronic properties of multi-junction ZnS/CdS/CdTe graded bandgap solar cells. *Mater. Chem. Phys.* **191**, 145–150 (2016). <https://doi.org/10.1016/j.matchemphys.2017.01.027>
  15. A.A. Ojo, W.M. Cranton, I.M. Dharmadasa *Next Generation Multilayer Graded Bandgap Solar Cells* (Springer, Cham, 2019). ISBN 978-3-319-96666-3
  16. A. Rockett, *The Materials Science of Semiconductors* (Springer, Boston, 2008). ISBN 978-0-387-25653-5
  17. I.M. Dharmadasa, Recent developments and progress on electrical contacts to CdTe, CdS and ZnSe with special reference to barrier contacts to CdTe. invited review paper. *Prog. Cryst. Growth Charact.* **36**(4), 249–290 (1998)
  18. I.M. Dharmadasa, G.J. Tolan, M. Cazaux, Effects of defects in semiconductors on reproducibility and performance of thin-film photovoltaic solar cells. *Semicond. Sci. Technol.* **23**, 10 (2008). <https://doi.org/10.1088/0268-1242/23/3/035023>
  19. I.M. Dharmadasa, Fermi level pinning and effects on CuInGaSe<sub>2</sub>-based thin-film solar cells. *Semicond. Sci. Technol.* **24**, 055016 (2009). <https://doi.org/10.1088/0268-1242/24/5/055016>
  20. I.M. Dharmadasa, A.P. Samantilleke, N.B. Chaure, J. Young, New ways of developing glass/conducting glass/CdS/CdTe/metal thin-film solar cells based on a new model. *Semicond. Sci. Technol.* **17**, 1238–1248 (2002). <https://doi.org/10.1088/0268-1242/17/12/306>
  21. I.M. Dharmadasa, J.S. Roberts, G. Hill, Third generation multilayer graded bandgap solar cells for achieving high conversion efficiencies—II: experimental results. *Sol. Energy Mater. Sol. Cells* **88**, 413–422 (2005)
  22. A.A. Ojo, I.M. Dharmadasa, 15.3% efficient graded bandgap solar cells fabricated using electroplated CdS and CdTe thin films. *Sol. Energy* **136**, 10–14 (2016). <https://doi.org/10.1016/j.solener.2016.06.067>
  23. I.M. Dharmadasa, *Advances in Thin-Film Solar Cells*, 2nd edn. (Pan Stanford, Singapore, 2018). ISBN 978-981-4800-12-9; 978-0-429-00124-6\$4